J. Appl. Comput. Mech., 7(4) (2021) 2149–2158
DOI: 10.22055/JACM.2020.33481.2234

ISSN: 2383-4536
jacm.scu.ac.ir

Shahid Chamran University of Ahvaz

Journal of Applied and Computational Mechanics

Research Paper

Size Effect on Inclined Cracking in Unidirectional Composites

Ahmet Abdullah Dönmez

Department of Civil Engineering, Istanbul Technical University, Maslak, Istanbul, 34469, Turkey

Received May 03 2020; Revised June 23 2020; Accepted for publication June 24 2020.
Corresponding author: A. Abdullah DÖNMEZ (donmezab@itu.edu.tr)

Abstract. The fracture and size effect properties of the unidirectional (UD) laminae were investigated based on the fracture energy analysis. The crack propagations on inclined fiber orientation may result in different energy release mechanisms. Therefore, the size effect behavior of these types of failures may vary according to the fracture parameters of the UD composites. This study aims to develop a fracture analysis of UD plies with inclined fibers relative to the loading axis. A numerical work with a developed material model was conducted to predict the size effect trends. The size effect law was used to fit the strength reduction with increasing size. The fundamentals of the quasibrittle fracture mechanics are shown to be applicable to analyze these types of structures. It is shown that the composite structures as quasibrittle materials, can exhibit a significant size effect.

Keywords: Size effect, fiber composite, quasibrittle fracture, inclined cracking.

1. Introduction

The fracture analyses of the structures are based on the microstructure of the members, whilst the global failure criteria mainly concern the external loads. Generally, the fracture analyses are thought to be based on the fracture energy methods while the global failure criteria are mainly related to the strength of materials concepts [1]–[3]. However, there are no differences between those two concepts concerning the equilibrium conditions. The strength of materials is a result and a particular case of the energy methods (fracture energy in the case of size effect).

The size effect is an essential feature of fracture mechanics. It is significant for fractures of quasibrittle materials, and cannot be identified by only the strength of materials concepts. With the presence of the size effect, the failure of composites cannot be predicted using only the stress or strain criteria. Because the strength criteria, which is the broadest design procedure, cannot take the size dependence into account. The size effect should be considered in the design of composite materials. The observed size effect is the deterministic size effect, which is based upon the release of the fracture energy and not only the statistical one which is the Weibullian size effect. The Weibullian type of size effect may exist but its influence can be neglected if the deterministic size effect occurs in the failure of a quasibrittle structure such as the fiber composites.

Several types of research on the size effect of the FRP composites exist in the literature [4]–[8]. But the most fundamental research regarding the theoretical and numerical work on the size effect on the branched cracks in a unidirectional (UD) fiber composite belongs to Dönmez and Bažant [5]. In [5], the branched cracking in a fiber composite is explained with the size effect concept. A strong size effect is found in the splitting (sideways) crack propagations. The strongest type of size effect refers to the asymptotic slope dictated by linear elastic fracture mechanics (LEFM). The LEFM dictates the brittle failures strengths being proportional to $D^{-1/2}$., where, D, corresponds to the characteristic size of the structure.

Figure 1 describes the problem in brief. If one considers a single edge notched UD composite under uniaxial tension, the propagation of the crack can develop in either the forward direction or the direction of long fibers (transverse or sideways). If the fiber direction is the same as the loading direction, the crack can develop as forward or sideways (splitting cracks) (see Fig. 1a). The splitting (or sideways) crack propagation can develop on one side or both sides depending on the geometry and mechanical properties of the structure. Here the calculations are based on one-sided crack growth in the sideway direction. The cracks usually follow the fiber orientation to develop in a strongly orthotropic composite. Therefore, inclined cracks occur if the strong axis of a UD composite is not perpendicular to the crack alignment but oriented with an oblique angle as shown in Fig. 1b. In these cases, the competing toughness mechanisms tend to be governed by the weak planes along with the fiber inclination. Finally, the size effect method, used in this study, is described in Fig. 1c, where the crack lengths and specimen dimensions are scaled accordingly.

The crack propagation based on the fiber alignment may result in different energy release mechanisms and the energy release rate ($\mathcal{G}$). The energy release rate is the fundamental concept of equilibrium in fracture propagation, introduced in 1921 by Griffith [9] then developed by Irwin [10]. The gray shaded areas in Fig. 1 represent the relieved-stress regions caused by the crack propagations. The values of $\mathcal{G}$ can be calculated based on these gray shaded areas. In the case of inclined crack propagation, the stress relief zones may be bounded by different slopes (k). These lines are approximations for the separation of the regions where the energy is released. In real the transition from the strain energy regions to the stress relief regions is gradually evolving. But the stress diffusion lines concept is shown to be a good approximation for solving the fracture problems if one defines k realistically [4], [5], [11].

Published online: September 02 2021

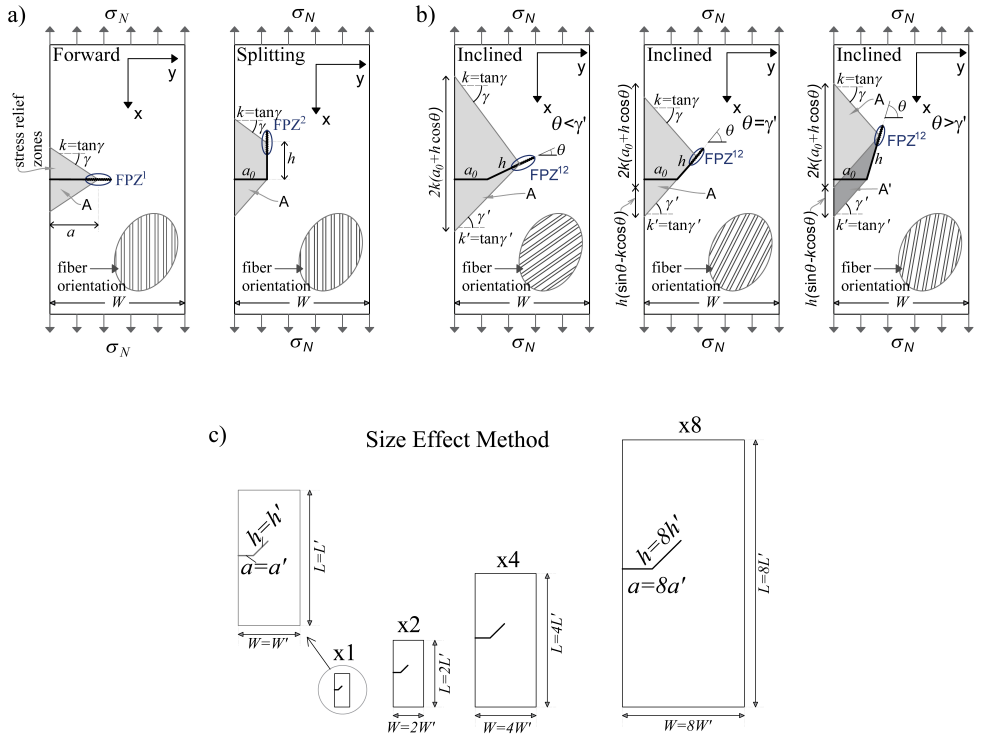

Fig. 1. Crack propagation types based on different fiber orientations, and corresponding energy release zones (gray areas) for a) forward and splitting (sideways) cracks, b) inclined cracks (dark black lines refer to the cracks), and c) the scaled UD specimens for the size effect method.

To formulate the energy release rate, strain energy density for the fracture energy calculation, can be used. The first derivative of the total strain energy of the gray areas in Fig. 1 with respect to the crack length (a) yields the energy release rate ($\mathcal{G}$). The critical point of the energy release rate propagates the crack in the weakest direction. Regarding the forward propagation, the energy release rate equations for uniaxial stress states (Fig. 1) and unit thickness (b=1) can be stated as eq. (1):

$$u = \frac{\sigma_N^2}{2\bar{E}};\ U = uA; A = ka^2 \tag{1}$$

$$\mathcal{G} = \frac{\partial U}{\partial a} = \frac{\sigma_N^2}{2\bar{E}} 2ka = \Gamma_f \tag{2}$$

$$\sigma_N = \sqrt{\frac{\bar{E}\Gamma_f}{ka}} \tag{3}$$

where u stands for the strain energy density, $\bar{E}$ for the effective elastic modulus of the lamina, U for the total strain energy of the gray shaded zone, A for the gray shaded area in Fig. 1a (forward propagation), and a for the crack length. As shown in eq. (2), during the crack propagation, the energy release rate equals the fracture energy Γ_f (subscript f refers to the forward cracking). Equation (3) can be interpreted as the size dependence of the nominal strength of the lamina. The strength is proportional to $a^{-0.5}$, and a equals to the sum of a_0 and a_f, where a_0 is the initial crack length and a_f is a material constant almost equals to the 1/2-1/3 the length of fracture process zone (FPZ). For the splitting cracks the energy release rate and nominal strength derivations are shown below:

$$A = \left(a_0 h + 2\frac{a_0^2 k}{2}\right) \tag{4}$$

$$\mathcal{G} = \frac{\partial U}{\partial h} = \frac{\sigma_N^2}{2\bar{E}} a_0 = \Gamma_s \tag{5}$$

$$\sigma_N = \sqrt{\frac{2\bar{E}\Gamma_s}{a_0}} \tag{6}$$

where h refers to the splitting crack height and Γ_f to the fracture energy during the crack growth (for one-sided growth). Note that the partial derivation is taken with respect to the h and not to a. The main difference between the eq. (6) and eq. (3) is that for splitting cracks, nominal strength is independent of h, and a_f. Therefore, the splitting cracking of the lamina has the strongest form of the size effect. In a scaled structure, the strength is proportional to the $D^{-1/2}$. Here the characteristic size is defined as D= a_0. This type of size dependence is also dictated by the LEFM.

In the case of non-orthogonal crack growth in an inclined fiber direction, such as in Fig. 1b and one of the main concerns of the current paper, has slightly different forms than the equations for forward and sideway cracking. The triangles surrounding the stress relief zones have different slopes, which are k and k' as shown in Fig. 1b. However, deriving the fracture energy and strength relations requires simplifications. Therefore, to determine the size effect dependence of an inclined crack, the k and k' will be

assumed to be the same. Let the crack inclination be β and the angles of the stress diffusion lines be γ and γ' for the upper- and lower-sides respectively (see Fig. 1b). Here $\gamma$is assumed as equal to γ'. If $\theta \leq \gamma$ the gray shaded area grows on both sides of the cracking path. But the stress diffusion lines develop one-sided when $\theta > \gamma$.

$$A_T = A + A' = k\left(a_0 + h\cos\theta\right)^2 + \sin\theta + k\cos\theta\left(0.5h^2\cos\theta + ha_0\right) \tag{7}$$

$$\mathcal{G} = \frac{\partial U}{\partial h} = \frac{\sigma_N^2}{2\bar{E}}\frac{\partial A_T}{\partial h} = \frac{\sigma_N^2}{2\bar{E}}\left(h\cos\theta + a_0\right)\left(2k\cos\theta + \left\langle \sin\theta - k\cos\theta \right\rangle\right) = \Gamma_i \tag{8}$$

$$\sigma_N = \sqrt{\frac{2\bar{E}\Gamma_i}{\left(h\cos\theta + a_0\right)\left(2k\cos\theta + \left\langle \sin\theta - k\cos\theta \right\rangle\right)}} \tag{9}$$

Equations (7)-(9) illustrate the calculations of the energy release rate and nominal strength of the UD lamina with inclined fiber orientation. The Macaulay brackets manage the variation of the gray shaded area calculation in Fig. 1b (A' vanishes when $\theta \leq \gamma$). The energy release rate and nominal strength depend on h, θ, k, and a_0. The dependence of inclined crack propagation on many variables and discontinuous function form makes the problem complicated.

Another complication may arise if one considers the incremental growth of the crack which refers to the material constant of h_f. This parameter is almost equal to 1/3 to 1/2 the length of the FPZ. The fracture process zones may differ substantially depending on the stress state around the crack tip and material properties on the propagation path. In sideway crack propagation, the fracture is mainly governed by the shear stress though the normal stresses are not negligible. On the other hand, in forward crack propagation, the fracture is in Mode I (see Fig. 2).

Building a simplistic relation for the dependence of the strength on the size is not straightforward due to the various parameters affecting the energy release rate and nominal strength of a UD composite with inclined crack. Therefore, it is convenient to construct a reliable numerical form for the aforementioned problem. To do so, the crack band model [12] with elastic and failure criteria are employed to capture the size effect trend precisely. This study mainly deals with revealing the size effect trend of inclined crack propagation in a UD composite, depending on the secondary variables and as an extension to the previous work of Dönmez and Bažant [5].

2. Developing the Numerical Model

Bažant's one of the significant contributions to the applied and computational mechanics community, the crack band model, is originated in the 1980s [4], [12], [13]. The crack band model is unlike, and more general than, the cohesive crack model. Because the cohesive crack model [14], [15], as a line crack model using a scalar relation between stress and crack mouth opening displacement, cannot predict inclined cracking, unless a potential pre-crack path is introduced where the fracture is expected. Several recent examples of this type of crack modeling are done by [16], [17]. Though, this type of modeling requires the prediction of crack propagation and cannot be a general procedure for modeling the random cracking evolution. Predicting the development of an inclined propagation from the FPZ zone entails quasibrittle fracture mechanics. Different from cohesive crack model, it includes the tensorial damage in the FPZ at the crack tip. The simplest form of the quasibrittle fracture mechanics, which will be used in the current study, is the crack band model. The crack band model has been successfully utilized for the fiber composites in several works[18]–[20]. The basic idea of the crack band model for strain-softening in tension and shear is to dodge spurious mesh-sensitivity via altering the material parameters that govern the steepness of the softening post-peak stress-strain relation and define smeared cracking. With the crack band model, the dissipated fracture energy per the crack band length is approximately independent of the element size. The calibration is made by altering the material parameters depending on the element size. This type of adjustment also prevents excessively localized strain problems. Let the size of the finite element be h_e. If the strength criterion meets, a sudden stress drop would dissipate energy, which equals to the fracture energy of the material. For different structure sizes, if the element size (h_e) kept constant for all sizes, any further parameter calibration would not require capturing the appropriate fracture energy of the structures. This is the simplest way of using the crack band model and will be adopted here. The width of the crack band should be constant due to the strain localization restrictions of the failed elements. Therefore, the mesh-discretizations should comply with the crack inclination.

2.1 Elastic Constants of the UD Composites

First of all, the elastic constitutive model should be constructed properly. We consider orthotropic fiber lamina with UD reinforcement in the x-direction. Here the x and y directions correspond to the Lagrangian (global) coordinate systems, while 1 and 2 directions the material (or natural) coordinates. And the formulation is valid up to the strength thresholds. The plane stress formulation of the constitutive model can be written as below:

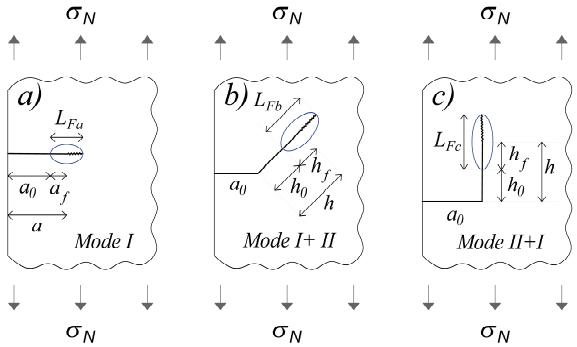

Fig. 2. The Fracture Process Zones (FPZ) for a) forward, b) inclined, and c) sideway crack formation.

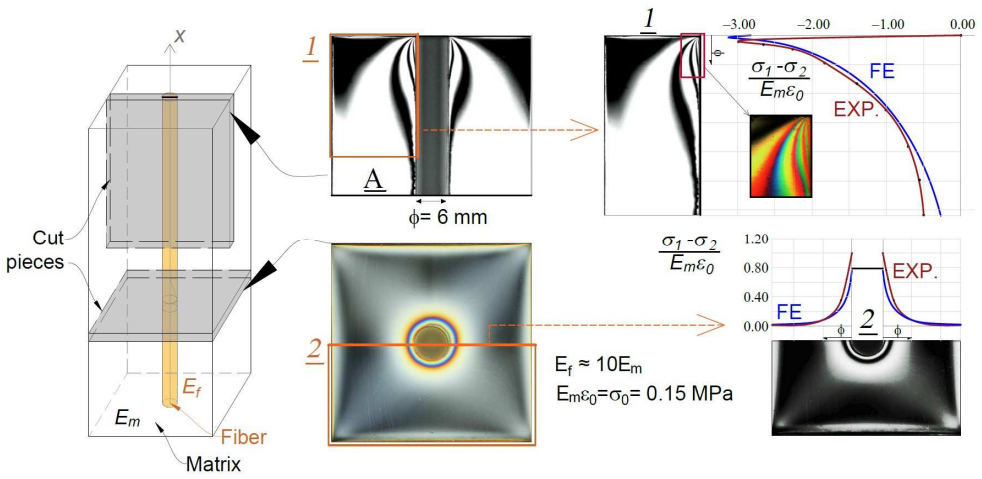

Fig. 3. The illustration of the rigid inclusion into a matrix continuum and corresponding stress patterns around the discontinuous singularity regions.

$$\begin{bmatrix}\sigma_{xx}\\ \sigma_{yy}\\ \tau_{xy}\end{bmatrix}=\begin{bmatrix}E_{xx} & E_{xy} & 0\\ E_{xy} & E_{yy} & 0\\ 0 & 0 & G_{xy}\end{bmatrix}\begin{bmatrix}\varepsilon_{xx}\\ \varepsilon_{yy}\\ \gamma_{xy}\end{bmatrix} \tag{10}$$

$$E_{xx}=\frac{E_1}{1-\nu_{12}\nu_{21}};E_{yy}=\frac{E_2}{1-\nu_{12}\nu_{21}};E_{xy}=\frac{\nu_{21}E_1}{1-\nu_{12}\nu_{21}};G_{xy}=G_{12} \tag{11}$$

where σ_{xx}, σ_{yy} = normal stresses in longitudinal and transverse directions, $_{xy}$ = shear stress, ε_{xx}, ε_{yy} = normal strains and $\gamma_{xy} = 2\varepsilon_{xy}$ = shear angle. Equations (10) and (11) are the plane stress constitutive relations of a transversely isotropic composite lamina which involves four elastic constants. Note that for the Poisson's ratios (ν_{12} and ν_{21}), the first subscript denotes the loading direction while the second subscript the strain direction. The equations shown above are very well-known relations of the macromechanics of the UD composite. Obtaining the elastic parameters of E_1, E_2, ν_{12}, ν_{21}, and G_{12} is a more tedious problem related to the micromechanics of the composites.

Micromechanical analysis can be complex because the stress singularity zones may arise in numerous regions at any of the discontinuous regions in the fiber composites [21]. The singularity concept can best be visualized by using photoelastic methods. As an illustration of the inclusion problem in a continuum medium, photoelastic modeling is used. An inclusion problem is solved using the frozen-stress method of photoelastic modeling. The disturbance is employed with the pre-strain application as the frozen-strain of the matrix material which is the birefringent epoxy. The cylindrical PA (polyamide) inclusion is glued to the prestrained epoxy matrix to ensure the isostrain situation. Cutting the photoelastic model with slices makes it possible to measure the stress profiles with the fringe pattern calculations [22], [23]. The obtained stress values can be regarded as the Tresca stresses since the conversion relations deduce the difference of the maximum and minimum principal stresses (σ_1-σ_2). The resulting stress profiles obtained for the normalized stress (normalized according to the prestress value in the matrix) are shown in Fig. 3.

Figure 3 is a generic representation of any inclusion problems like UD plies disturbed by any external forces. This type of representation, of course, cannot completely reflect the real mechanisms in the laminates. However similar singular point regions and corresponding stress profiles are assumed to exist in all types of inclusion problems. From a mathematical point of view, the singular points (or regions) are the zones where the stress values grow infinitely. However, the material plasticity would blunt the crack tip with the local yielding behaviors. Yet the non-homogenous stress values would ease the failure with germination the main crack from one of these points.

Analysis cannot be based on these microscales unless gross simplifications are taken into account. More comprehensive micromechanical models, constructed based on the elasticity theory, should be utilized to acquire the elastic engineering constants of fibrous composites. For very good estimates, the Hill-Hashin-Christensen-Lo formulae are employed for the elastic constants of UD lamina [24]–[27]. Equations are shown as below:

$$E_1=V_fE_f+V_mE_m+\frac{4\left(\nu_f-\nu_m\right)^2V_f\left(1-V_f\right)}{\frac{V_f}{k_m}+\frac{1-V_f}{k_f}+\frac{1}{G_m}} \tag{12}$$

$$E_2=\frac{2}{\frac{0.5}{K_L}+\frac{0.5}{G_{23}}+\frac{2\nu_{12}^2}{E_1}} \tag{13}$$

$$G_{12}=G_m\frac{\left(G_f+G_m\right)+V_f\left(G_f-G_m\right)}{\left(G_f+G_m\right)-V_f\left(G_f-G_m\right)} \tag{14}$$

$$\nu_{12} = V_f \nu_f + V_m \nu_m + \frac{(\nu_f - \nu_m) V_f (1 - V_f)}{\frac{V_f}{k_m} + \frac{1 - V_f}{k_f} + \frac{1}{G_{12}}} \left(\frac{1}{k_m} - \frac{1}{k_f} \right) \tag{15}$$

$$k_f = \frac{E_f}{3(1 - 2\nu_f)}; k_m = \frac{E_m}{3(1 - 2\nu_m)} \tag{16}$$

$$K_L = k_m + \frac{G_m}{3} + \frac{V_f}{\frac{1}{k_f - k_m + (G_f - G_m)/3} + \frac{1 - V_f}{k_m + 4G_m/3}} \tag{17}$$

$$G_{23} = G_m \left(1 + \frac{V_f}{\frac{G_m}{(G_f - G_m)} + \frac{(k_m + 7G_m/3)(1 - V_f)}{2k_m + 8G_m/3}} \right) \tag{18}$$

where the subscripts m refers to the matrix, f to the fiber, 1 to the strong direction (or fiber direction), and 2 to the transverse direction (or the weak direction). Note that in these equations the matrix material is assumed isotropic. G denotes the shear modulus and in an isotropic material equals to the $E/(2(1+\nu))$. For the fiber material, the G_{f12} is calculated as $0.065E_f / (2(1+\nu_f))$.

2.2 Failure Criteria and Damage Parameters

Matzenmiller et al. (1995) used continuum damage mechanics coupled with failure criteria for the anisotropic materials [28]. This method is adopted here, and the damage tensor $\boldsymbol{D}$ is utilized for the transition of stresses between the undamaged ($\boldsymbol{\sigma}$) and damaged ($\hat{\boldsymbol{\sigma}}$) material. Employing the damage into the stress values are shown as below:

$$\hat{\boldsymbol{\sigma}} = \boldsymbol{D}\boldsymbol{\sigma} \tag{19}$$

$$\boldsymbol{\sigma} = \begin{bmatrix} \sigma_{xx} \\ \sigma_{yy} \\ \tau_{xy} \end{bmatrix}; \boldsymbol{D} = \begin{bmatrix} d_{11} & 0 & 0 \\ 0 & d_{22} & 0 \\ 0 & 0 & d_{12} \end{bmatrix}; \hat{\boldsymbol{\sigma}} = \begin{bmatrix} \hat{\sigma}_{xx} \\ \hat{\sigma}_{yy} \\ \hat{\tau}_{xy} \end{bmatrix} \tag{20}$$

The damage variables d_{11}, d_{22}, and d_{12} are the functions of the strains. The limit strain values can be found by using Hashin's criteria: (Hashin 1980) [29].

$$\text{for}(\sigma_{xx} > 0): \frac{\varepsilon_{xx}}{e_{ft}} < 1 \tag{21}$$

$$\text{for}(\sigma_{xx} < 0): \left| \frac{\varepsilon_{xx}}{e_{ft}} \right| < 1 \tag{22}$$

$$\text{for}(\sigma_{yy} > 0): \left(\frac{\gamma_{xy}}{\gamma_m} \right)^2 + \left(\frac{\varepsilon_{yy}}{e_{mt}} \right)^2 < 1 \tag{23}$$

$$\text{for}(\sigma_{yy} < 0): \left(\frac{\gamma_{xy}}{\gamma_m} \right)^2 + \left(\frac{\varepsilon_{yy}}{e_{mc}} \right)^2 < 1 \tag{24}$$

where e_{ft}, e_{mc}, e_{mt} and γ_m refer to tensile strain limits of the fibers and the threshold values of compressive, tensile, and shear strains of the matrix, respectively. Equation (21) depends on fiber strength and Eqs. (22)-(24) depend only on the matrix parameters.

The damage variables d_{11}, d_{22}, and d_{12} can be calculated as in Eqs. (25)-(31).

$$\text{for}(\sigma_{xx} > 0): d_{11} = \exp\left(-c_f \frac{\varepsilon_{xx}}{e_{ft}} - 1 \right) \tag{25}$$

$$\text{for}(\sigma_{xx} > 0): d_{11} = \exp\left(-c_m \left| \frac{\varepsilon_{xx}}{e_{mc}} \right| - 1 \right) \tag{26}$$

$$\text{for}(\sigma_{yy} > 0): d_{22} = \exp\left(-c_m c_{sy} \left(\frac{\gamma_{xy}}{\gamma_m} \right)^2 + \left(\frac{\varepsilon_{yy}}{e_{mt}} \right)^2 - 1 \right) \tag{27}$$

$$\text{for}\left(\sigma_{yy}>0\right):\ d_{12}=\exp\left(-c_m\left(\frac{\gamma_{xy}}{\gamma_m}\right)^2+\left(\frac{\varepsilon_{yy}}{e_{mt}}\right)^2-1\right) \tag{28}$$

$$\text{for}\left(\sigma_{yy}<0\right):d_{22}=\exp\left(-c_m c_{sy}\left(\frac{\gamma_{xy}}{\gamma_m}\right)^2+\left(\frac{\varepsilon_{yy}}{e_{mc}}\right)^2-1\right) \tag{29}$$

$$\text{for}\left(\sigma_{yy}<0\right):\ d_{12}=\exp\left(-c_m\left(\frac{\gamma_{xy}}{\gamma_m}\right)^2-c_{sy}\left(\frac{\varepsilon_{yy}}{e_{mc}}\right)^2-1\right) \tag{30}$$

where c_f, c_m, c_{sy}, and c_{ys} are the factors linked to the softening behavior of fiber rupture, matrix compressive failure, the coupling of shear with matrix tensile failure, and coupling of matrix tension with shear failure, respectively. Note that there are of course several assumptions and simplifications associated with the derivation of the damage parameters of d_{11}, d_{22}, and d_{12}.

In the damage and failure relationships, the kinging (or buckling) of the fibers is ignored. Thus, in compressive failures, the only damage parameters are related to the matrix material in any direction. The failure in the transverse direction, direction 2 in the material orientation, is governed by the matrix material. The coupling between the shear and tension actions is characterized by the parameter c_{sy} in Eqs. (25)-(30). The minus $-c_{ys}$ in eq. (30) is due to the positive effect of compression on the shear strength. The softening behavior of the fiber rupture is much steeper than the failure of the matrix material. Interaction of shear-tension and shear-compression failure types are not bilaterally equal. The influence of shear stress on the normal stress failures is much less than the effect of normal stress on the shear failures.

The damage parameters should, also, apply to the stiffness of the material. Therefore, the damage of the elastic constants can be implemented as in Eqs. (31)-(32).

$$\hat{E}_{xx}=\frac{d_{11}E_1}{1-d_{11}d_{22}\nu_{12}\nu_{21}};\ \hat{E}_{yy}=\frac{d_{22}E_2}{1-d_{11}d_{22}\nu_{12}\nu_{21}} \tag{31}$$

$$\hat{E}_{xy}=\frac{d_{11}d_{22}\vartheta_{21}E_1}{1-d_{11}d_{22}\nu_{12}\nu_{21}};\ \hat{G}_{xy}=d_{12}G_{xy} \tag{32}$$

where the $\hat{\mathbf{E}}$ denotes the tensor of the elastic constants of the damaged material. There might be one more process to complete the full derivation of the FE model. The characteristics of the stress-strain curve of a matrix are generally nonlinear. The most common polymer matrix is epoxy which is one of the thermosetting polymers. The mechanical behavior under uniaxial stress state is nonlinear elastic. However linear assumptions might not lead to gross errors. On the other hand, the shear stress- shear angle curve of epoxy is highly nonlinear [30]. Modeling this behavior requires special treatment. For the shear modulus of the matrix material, the following relationship might be used to capture this nonlinearity.

$$G_{xy}=G_{m0}-\xi\gamma_{xy} \tag{33}$$

where G_{m0} is the shear modulus of the matrix with zero strain. The ξ parameter is a free parameter that needs to be determined based on the experimental data. For a crude estimate, ξ can be taken as 10000 depending on the nonlinearity level of the shear response of epoxy.

3. Numerical Results

The numerical work in this study consists of the FE analysis. A commercial FE software, ABAQUS, was used for the simulations. The numerical framework involves validations of the aforementioned equations and predictions based on the calibration of the model by using the tests from the literature. The explicit numerical algorithm was used for the simulations. Plane stress conditions were followed for all the simulations. So, 4-nodes shell elements were selected in the FE implementations. The material modeling, shown in the preceding sections, was adapted by means of a user subroutine VUMAT. The quasi-static loading conditions were ensured by keeping the loading rate sufficiently small compared to the wave speeds of stress inside the smallest element. The element size was kept constant for each calibrated data set. The element size was kept to ensure the crack band model concept regarding the released energy match per failed element. The material inclination angles or the fiber orientations were applied inside the composite layup option.

The validation of the FE model in terms of the elastic constants was performed using the off-axis tests of Zhao et al. (2018) [30]. In these tests, the unnotched UD laminae with different material orientations were undergone uniaxial stress until the failure. The UD prepregs have 0.125mm thickness. Specimens contain 62% carbon fiber in volume fraction. The tested and simulated specimens involve 7 different orientation angles (β). The results of the simulations are shown in Fig. 4. Figure 4 illustrates the level of the nonlinearity of the material depending on the material orientations. The lack of linearity is visible for the angles between β=0° and 45°. Equation (31) can capture this nonlinearity for the β=15° and 30° inclinations. The Hill-Hashin-Christensen-Lo formula for the elastic constants was shown to estimates the material response for the β=0° and 90° orientations while slight modifications are needed for the shear governed failures.

To calibrate the aforementioned models the failure and damage criteria with the elastic constants were validated with the 2nd test data belong to Catalanotti et al [31]. The tests include quasi-isotropic and cross-ply laminates of different sizes. The scaling of the material should obey the 2D geometrical scaling laws. Therefore, the thickness of the specimens was kept constant. The FE computations of the size effect experiments were conducted for both quasi-isotropic and cross-ply laminates. In either case, the authors used double-edge notched specimens under uniaxial loading. The scaled sizes are W=10, 15, 20, 25, 30, 35 mm for quasi-isotropic (QI) laminates and W=10, 15, 20, 25, 30, 35 mm for cross-ply (CP) laminates. Where W corresponds to the total width of the tensile specimen. Bažant's size effect law (SEL) [4] was used in the study, which is also stated in Eq. (34). The proposed FE model can fit the experimental data as shown in Fig. 5a, b. The quasi-isotropic specimens exhibited more brittle behavior compared to the cross-ply laminates. According to the SEL fit with the computed data, transitional size (D_0) is smaller than the cross-ply laminates. It is noteworthy to mention that the sideways cracking in cross-ply laminates reduces the stress concentrations on the initial crack tip (Fig. 5c, d).

Table 1. Parameters used in the numerical study in Fig. 6.

V_f	E_f [MPa]	E_m [MPa]	ν_f	ν_m	e_{ft}	e_{mt}	e_{mc}	γ_m	ξ	c_f	c_m	c_{sy}	h_e [mm]
60%	282000	3200	0.25	0.25	0.0176	0.025	0.026	0.042	10000	0.9	0.0002	0.5	1.00

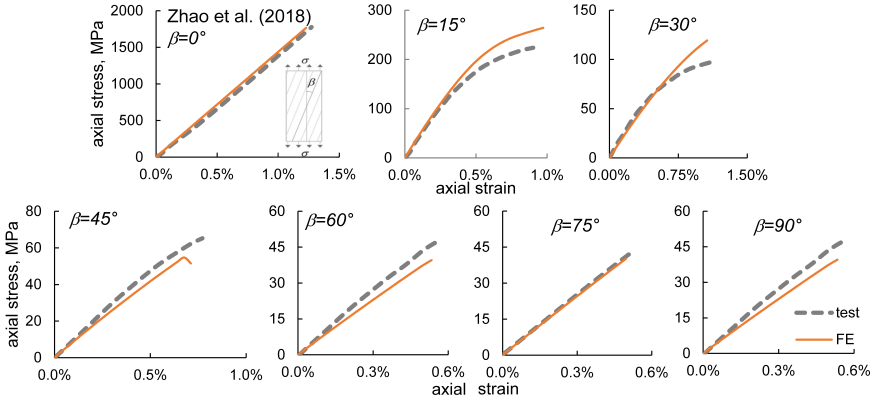

Fig. 4. Results of the elastic model using the off-axis tests of [30].

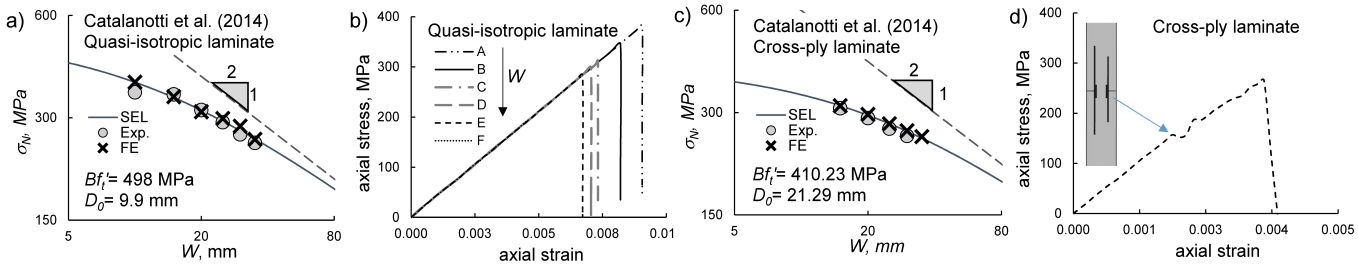

Fig. 5. Size effect analysis of a, b) quasi-isotropic, c, d) cross-ply laminates. Calibrated by the test data of [31].

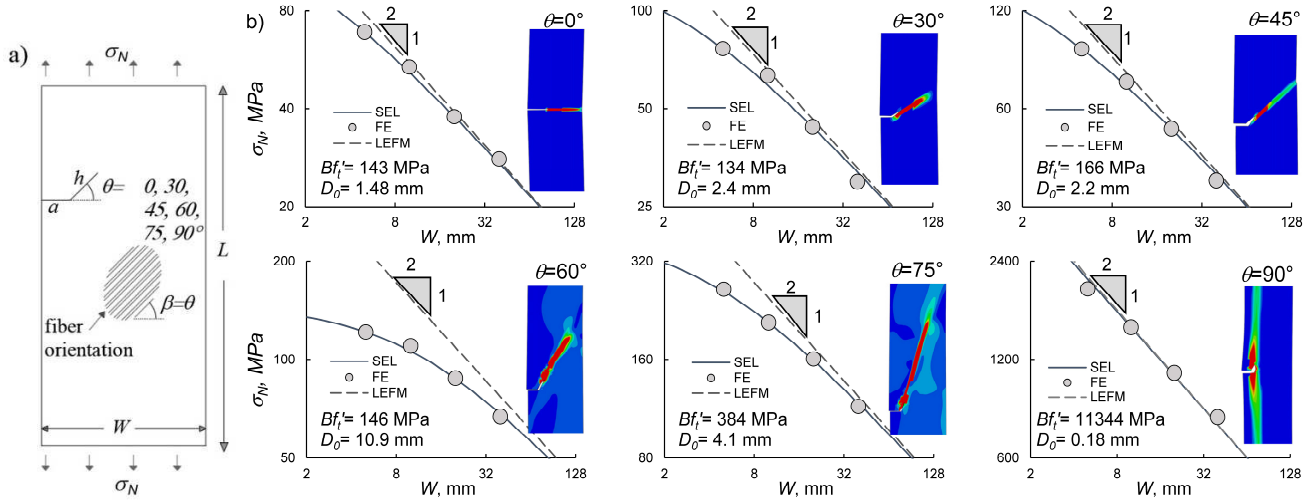

Fig. 6. a) The virtual specimen for the FE analysis and b) size effect analyses results of the specimens for four different sizes.

$$\sigma_N = \frac{Bf_t'}{\sqrt{1+\frac{D}{D_0}}} \quad \text{(SEL)} \tag{34}$$

$$Bf_t' = \frac{K_{IC}}{\sqrt{g_0 h_f}};\ D_0 = \frac{g_0'}{g_0} h_f \tag{35}$$

where K_{IC} is the critical value of the stress intensity factor or the fracture toughness, g_0 is a correction factor defined as the dimensionless energy release function, depending on the geometry of the specimen.

Table 2. Obtained parameters from J-integral and Eqs. (8), (34) and (35).

θ (=β)	0°	30°	45°	60°	75°	90°
$\mathcal{G}_c$ [N/mm]	2.33	1.54	1.11	1.32	0.86	13.52
Ê [MPa]	4656.01	6184.91	9159.80	17473.50	51485.10	170489.46
k	6.91	6.12	6.44	6.85	10.20	NA
γ	81.76°	81.41°	81.17°	81.69°	84.40°	NA
g_0	0.35	0.27	0.19	0.13	0.08	NA
g_0'	0.49	0.32	0.20	0.09	0.03	NA
h_f (a_f) [mm]	1.04	2.00	2.10	15.52	10.58	NA

Based on the validation and calibration conducted with the experimental data of [30], [31], which are also shown in Figs. 4 and 5, the size effect predictions for the UD laminates with different fiber orientations were implemented. The size of the elements used in numerical work is 1 mm. Because of the crack band model requirements, this element size kept constant with the other parameters shown in Table 1. The threshold values may change according to the material characteristics. But the damage evolution can be captured with the parameters of c_f, c_m, and c_{sy}. These parameters were defined according to the calibration of the test results of [31], which is shown in Fig. 5. For the FE analysis, a virtual specimen with a single edge notch exposed to the uniaxial tension was modeled as illustrated in Fig. 6a. The selected model has an L/W ratio 16 where the L is the length of the specimen and W is the width. The ratio of the initial (main) crack to the width, a/W, equals 1/5. As a secondary crack (or the daughter crack), the kinked crack's length h in Fig. 6a, also shown in Figs. 1 and 2, equal to the length of a. The orientation of the kinked crack (θ) is the same as the orientation of the material axis (β). So, the crack growth can align with the strong direction, which is the direction of the fibers. For the size effect analysis, the dimensionless parameters of a=h and θ=β, and the ratios of a/W and W/L should be kept constant for different sizes. Based on the plane stress analysis, geometrically scaling of the specimens should follow the 2D scaling law. The smallest specimen has a width of W=5 mm. Four different sizes were used to keep the element size the same to implement the crack band model and to keep the fracture energies the same per one element's failure. Six different fiber orientations, which are 0°, 30°, 45°, 60°, 75°, and 90°, were used in the size effect analysis. The obtained results are shown in Fig. 6b.

Figure 6b illustrates the size effect results of the virtual specimens for six different fiber orientations (or kinked crack orientation). The analysis includes four different scaled sizes, W= 5, 10, 20, and 40 mm. The solid circles denote the nominal strengths which are calculated as the maximum load divided by the cross-sectional area ($P_{max}/(Wb)$), where b is the thickness of the specimen and in the plane stress analysis should be taken as unity. However, the definition of P_{max} is different for θ=90°, which is the splitting (sideways) cracking. In the case of θ=90°, the P_{max} should be decided with great care since the load will continue to increase after the sideways crack growth. However, the load usually exhibits a slight drop on the load-deflection curve depending on the geometry in the displacement-controlled tests. This load drop location should be taken as the P_{max} in the splitting strength definitions, which was also done in [5].

The solid lines in Fig. 6b refer to Bažant's size effect law (SEL in eq. (34)). The nonlinearity level of the fracture behavior can be inferred from the size effect fits. This level also demonstrates the deviations from the LEFM slope of -1/2, which is shown as the dashed lines in Fig. 6b. It can be seen that the deviation from LEFM initially decreases then increases as the fiber orientation changes from 0° to 90°. When the crack propagates sideways direction, the exhibited size effect trend has a slope of -1/2 (LEFM type) which corresponds to a very small transitional size (D_0) for the 90° inclination. This result complies with the eq. (8) and the results of [5]. The resulting cracking patterns illustrated by the principal strain components are also depicted in Fig. 6b. The cracking pattern is obtained from the strain values after the peak-load corresponding to various fiber orientations aligned with the material's strong direction. This type of crack-path, which depends on the fiber orientation, conforms to the experimental evidence such as [32]–[34].

It can be seen from Fig. 6 that, the transitional size (D_0) is non-monotonic which is a parameter that depends on both the material and shape. As a rough approximation, D_0 is proportional to the FPZ length and critical effective crack extension, h_f or a_f, (in other words effective FPZ length). Therefore, the highest value of D_0 for the 60° inclination might be the result of the high FPZ length for that orientation. In order to calculate the effective FPZ lengths (h_f or a_f), the critical value of the energy release rates ($\mathcal{G}_c$), dimensionless energy release rate (g_0), and the derivative of the g_0' with respect to crack length, can be calculated by means of the J-integral method, which is already a built-in tool of the ABAQUS software, under uniaxial stress state and eqs. (34) and (35). Since the values for a and h are known for the problem of interest, the k and γ can be obtained with the help of eq. (8). The results of the J-integral analysis for the problem and calculated parameters are shown in Table 2. The stress diffusion lines are not changing considerably with the crack orientation. For 90 orientation the $\mathcal{G}$ is independent of k hence the values of k and γ are not given in Table 2. The case of 60° orientation has the highest effective FPZ length (h_f) which resulted in the highest transitional size parameter D_0.

4. Conclusion

The unidirectional laminates were analyzed using quasibrittle fracture mechanics. The stress relief zones and stress diffusion lines concepts were used to formulate the fracture mechanisms. A numerical framework was constructed to simulate the virtual UD fracture specimens. Bažant's size effect law was used to demonstrate the size dependence of the nominal strengths of inclined fiber composites. Some of the main conclusions can be drawn as below:

- The splitting cracking with a realistically defined peak load induces the asymptotic slope of -1/2 which is dictated by the LEFM. This behavior is demonstrated in eq. (8) and Fig. 6b for the case of θ=90°.
- A photoelastic model was used to demonstrate the regions of singularity where the fracturing may most likely germinate from. However, the elastic stiffness matrix requires simplifying the mechanisms of fiber composites. The elastic constants proposed by Hill-Hashin-Christensen-Lo was shown to estimate the elastic behavior of UD laminates with negligible errors.
- The UD composite specimens with various fiber orientation angles exhibit a strong size effect depending on the orthotropic and shape properties of the specimens. Bažant's size effect law (SEL) can fit the quasibrittle fracture mechanisms of the UD composites. The deviation from the LEFM slope varies according to the fiber inclination of the UD laminate under uniaxial tension loading.
- The highest level of nonlinear fracturing was observed in the case of 60° fiber (or crack) orientation angle among the simulated specimens as shown in Fig. 6b. The highest transitional size D_0 and longest effective FPZ length (h_f) were also obtained from the 60° angle, which may be due to the relatively long nonlinear damage zone.

Acknowledgments

The author thanks Zdenek P. Bažant for his mentoring and guidance during the author's post-doctoral trainee at Northwestern University.

Conflict of Interest

The author declared no potential conflicts of interest with respect to the research, authorship, and publication of this article.

Funding

The author received no financial support for the research, authorship, and publication of this article.

Data Availability Statements

The datasets generated and/or analyzed during the current study are available from the corresponding author on reasonable request.

Nomenclature

A	Area of stress relief zone [m^2]	h	Length of the inclined crack [m]
A_T	Total area of stress free zones in inclined cracking [m^2]	h_0	Initial length of inclined crack [m]
A'	The additional stress-free area in inclined crack [m^2]	h_e	Element (mesh) size [m]
a	Initial length of inclined crack [m]	h_f	Effective FPZ length for the inclined crack extension [m]
a_0	Length of inclined crack extension [m]		
a_f	Effective FPZ length for the horizontal crack extension [m]	K_{ic}	Critical value of stress intensity factor [MPa m$^{0.5}$]
		k	Slope of the stress diffusion line
B	Dimensionless constant	k'	Slope of the 2nd stress diffusion line (below the crack)
b	Thickness of specimen [m]	L_f	Length of the FPZ [m]
c_f	Numerical parameter controlling the fiber post-peak	U	Total elastic strain energy [Nm]
c_m	Numerical parameter controlling the matrix post-peak	u	Elastic strain energy density [J/m^3]
c_{sy}	Parameter controlling the coupling of normal and shear stress	V_f	Volume fraction of fiber
$\boldsymbol{D}$	The continuum damage tensor	V_m	Volume fraction of matrix
D	Characteristic length of the structure [m]	W	Width of the specimen [m]
D_0	The transitional size fracture parameter [m]	β	Angle of fiber orientation
d_{11}	Damage component in x-direction	ε_0	The pre-strain
d_{22}	Damage component in y-direction	ε_{xx}, ε_{yy}	Global direct strain components in x and y-directions
d_{12}	Damage component in shear direction	ε_{xy}	Global shear strain in tensorial components.
$\bar{E}$	Effective elastic modulus of material [MPa]	Γ_i	Fracture energy of inclined propagation [N/m]
E_1	Local (material) elastic component in 1-direction [MPa]	Γ_f	Fracture energy of forward propagation [N/m]
E_2	Local (material) elastic component in 2-direction [MPa]	Γ_s	Fracture energy of sideways propagation [N/m]
E_{xx},E_{yy},E_{xy}	Global direct elastic components [MPa]	γ	Angle of the slope of k
$\hat{E}_{xx}$,$\hat{E}_{yy}$,$\hat{E}_{xy}$,	Global damaged direct elastic components. [MPa]	γ'	Angle of the slope of k'
E_f	Elastic modulus of fiber [MPa]	γ_m	Shear strain threshold of matrix
E_m	Elastic modulus of matrix [MPa]	γ_{xy}	Shear angle or the engineering shear strain
e_{ft}	Strain threshold of fiber in tension	ν_{12}	Local Poisson's ratio (stress in 1-dir, strain in 2-dir)
e_{mt}	Strain threshold of matrix in tension	ν_f	Poisson's ratio of fiber
e_{mc}	Strain threshold of matrix in compression	ν_m	Poisson's ratio of matric
f_t'	Tensile strength [MPa]	θ	Angle of crack orientation
$\mathcal{G}$	Energy release rate [N/m]	$\boldsymbol{\sigma}$	Global stress tensor
$\mathcal{G}_{ft}$	Critical value of the energy release rate [N/m]	$\hat{\boldsymbol{\sigma}}$	Damaged stress tensor
G_{12}	Local (material) shear modulus 12-direction [MPa]	σ_1	First principal stress [MPa]
G_{23}	Local (material) shear modulus 23-direction [MPa]	σ_2	Second principal stress [MPa]
G_f	Shear modulus of fiber [MPa]	σ_N	Nominal strength of structure [MPa]
G_m	Shear modulus of matrix [MPa]	σ_{xx}	Global stress component in x-direction [MPa]
G_{m0}	Initial shear modulus of matrix [MPa]	σ_{yy}	Global stress component in y-direction [MPa]
G_{xy}	Global shear modulus [MPa]	τ_{xy}	Global shear stress component [MPa]
$\hat{G}_{xy}$	Global damaged shear modulus [MPa]	ξ	Numerical parameter controlling the nonlinearity of G_m
g_0	Dimensionless energy release rate		
g_0'	Derivative of g_0 with respect to a.		

References

[1] Arridge, R.G.C., Fracture of Fibre Reinforced Materials, *Nature*, 223, 1969, 941–943.
[2] Wang, Y., Chen, D., Li, N., Yuan, H., Zhu, Z., Li, Y., Huang, Z., A Micromechanics Based Elasto-Plastic Damage Model for Unidirectional Composites under off-Axis Tensile Loads, *Nature Research, Scientific Reports*, 10, 2020, 847.
[3] Anguita, J. V., Smith, C.T.G., Stute, T., Funke, M., Delkowski, M., Silva, S.R.P., Dimensionally and Environmentally Ultra-Stable Polymer Composites Reinforced with Carbon Fibres, *Nature Materials*, 19, 2020, 317–322.

[4] Bažant, Z.P., Planas, J., *Fracture and size effect in concrete and other quasibrittle materials*, Boca Raton, Boston, London: CRC press, 1997.
[5] Dönmez, A., Bažant, Z.P., Size Effect on Branched Sideways Cracks in Orthotropic Fiber Composites, *International Journal of Fracture*, 222, 2020, 155–169.
[6] Salviato, M., Kirane, K., Ashari, S., Bažant, Z.P., Cusatis, G., Experimental and Numerical Investigation of Intra-Laminar Energy Dissipation and Size Effect in Two-Dimensional Textile Composites, *Composites Science and Technology*, 135, 2016, 67–75.
[7] Salviato, M., Kirane, K., Bažant, Z.P., Cusatis, G., Mode I and II Interlaminar Fracture in Laminated Composites: A Size Effect Study, *Journal of Applied Mechanics*, 86, 2019, 9.
[8] Bažant, Z.P., Daniel, I.M., Li, Z., Size Effect and Fracture Characteristics of Composite Laminates, *Journal of Engineering Materials and Technology, Transactions of the ASME*, 118(3), 1996, 317–324.
[9] Griffith, A.A., VI. The Phenomena of Rupture and Flow in Solids, *Philosophical transactions of the royal society of london. Series A, containing papers of a mathematical or physical character*, 221(582–593), 1921, 163–198.
[10] Irwin, G.R., Onset of Fast Crack Propagation in High Strenght Steel and Aluminum Alloys, *Naval Research Laboratory*, 4763, 1956, 1–15.
[11] Dönmez, A., Bažant, Z.P., Critique of Critical Shear Crack Theory for Fib Model Code Articles on Shear Strength and Size Effect of Reinforced Concrete Beams, *Structural Concrete*, 2019, 20(4), 1451–1463.
[12] Bažant, Z.P., Oh, B.H., Crack Band Theory for Fracture of Concrete, *Matériaux et Construction*, 16(3), 1983, 155–177.
[13] Bažant, Z.P., Lin, F.B., Nonlocal Smeared Cracking Model for Concrete Fracture, *Journal of Structural Engineering*, 114(11), 1988, 2493–2510.
[14] Barenblatt, G.I., The Mathematical Theory of Equilibrium Cracks in Brittle Fracture, *Advances in Applied Mechanics*, 7(1), 1962, 55–129.
[15] Hillerborg, A., Modéer, M., Petersson, P., Analysis of Crack Formation and Crack Growth in Concrete by Means of Fracture Mechanics and Finite Elements, *Cement and Concrete Research*, 6(6), 1976, 773–781.
[16] Noselli, G., Deshpande, V.S., Fleck, N.A., An Analysis of Competing Toughening Mechanisms in Layered and Particulate Solids, *International Journal of Fracture*, 183(2), 2013, 241–258.
[17] Tankasala, H.C., Deshpande, V.S., Fleck, N.A., Notch Sensitivity of Orthotropic Solids: Interaction of Tensile and Shear Damage Zones, *International Journal of Fracture*, 212(2), 2018, 123–142.
[18] Pineda, E.J., Waas, A.M., Numerical Implementation of a Multiple-ISV Thermodynamically-Based Work Potential Theory for Modeling Progressive Damage and Failure in Fiber-Reinforced Laminates, *International Journal of Fracture*, 182(1), 2013, 93–122.
[19] Rudraraju, S., Salvi, A., Garikipati, K., Waas, A., In-Plane Fracture of Laminated Fiber Reinforced Composites with Varying Fracture Resistance: Experimental Observations and Numerical Crack Propagation, *International Journal of Solids and Structures*, 47(7–8), 2010, 901–911.
[20] Xu, W., Thorsson, S.I., Waas, A.M., Experimental and Numerical Study on Cross-Ply Woven Textile Composite with Notches and Cracks, *Composite Structures*, 132, 2015, 816–824.
[21] Pathan, M.V., Ponnusami, S.A., Pathan, J., Pitisongsawat, R., Erice, B., Petrinic, N., Tagarielli, V.L., Predictions of the Mechanical Properties of Unidirectional Fibre Composites by Supervised Machine Learning, *Scientific Reports*, 9, 2019, 13964.
[22] Abdulaliyev, Z., Ataoglu, S., Dönmez, A., Stress State of Pretensioned Structures, *Journal of Testing and Evaluation*, 48(5), 2020, 3768-3778.
[23] Donmez, A., Ataoglu, S., Abdulaliyev, Z., An Experimental Study on Pre-Tensioned Concrete Members, in *6th International Conference on Advances in Structural Engineering and Construction Management*, 2015, 41–46.
[24] Hill, R., Theory of Mechanical Properties of Fibre-Strengthened Materials—III. Self-Consistent Model, *Journal of the Mechanics and Physics of Solids*, 13(4), 1965, 189–198.
[25] Hashin, Z., On Elastic Behaviour of Fibre Reinforced Materials of Arbitrary Transverse Phase Geometry, *Journal of the Mechanics and Physics of Solids*, 13(3), 1965, 119–134.
[26] Christensen, R.M., Lo, K.H., Solutions for Effective Shear Properties in Three Phase Sphere and Cylinder Models, *Journal of the Mechanics and Physics of Solids*, 27(4), 1979, 315–330.
[27] Huang, Z., Zhou, Y., *Strength of Fibrous Composites*, Hangzhou: Zhejiang University Press, Springer, 2011.
[28] Matzenmiller, A., Lubliner, J., Taylor, R.L., A Constitutive Model for Anisotropic Damage in Fiber-Composites, *Mechanics of Materials*, 20(2), 1995, 125–152.
[29] Hashin, Z., Failure Criteria for Unidirectional Fiber Composites 1, *Journal of Applied Mechanics*, 47(2), 1980, 329–334.
[30] Zhao, Y.Q., Zhou, Y., Huang, Z.M., Batra, R.C., Experimental and Micromechanical Investigation of T300/7901 Unidirectional Composite Strength, *Polymer Composites*, 40(7), 2019, 2639–2652.
[31] Catalanotti, G., Arteiro, A., Hayati, M., Camanho, P.P., Determination of the Mode I Crack Resistance Curve of Polymer Composites Using the Size-Effect Law, *Engineering Fracture Mechanics*, 118, 2014, 49–65.
[32] Woo, S.C., Choi, N.S., Analysis of Fracture Process in Single-Edge-Notched Laminated Composites Based on the High Amplitude Acoustic Emission Events, *Composites Science and Technology*, 67(7–8), 2007, 1451–1458.
[33] Kaman, M.O., Effect of Fiber Orientation on Fracture Toughness of Laminated Composite Plates [0°/θ°]S, *Engineering Fracture Mechanics*, 78(13), 2011, 2521–2534.
[34] Beuth Jr., J.L., Gregory, M.A., Herakovich, C.T., Crack Growth in Unidirectional Graphite-Epoxy under Biaxial Loading, *Experimental Mechanics*, 26, 1986, 245–253.

ORCID iD

Ahmet Abdullah Dönmez https://orcid.org/0000-0002-2448-7090

How to cite this article: Dönmez A.A. Size Effect on Inclined Cracking in Unidirectional Composites, *J. Appl. Comput. Mech.*, 7(4), 2021, 2149–2158. https://doi.org/10.22055/JACM.2020.33481.2234